Supporting Information

Chung et al. 10.1073/pnas.1203707109

SI Text

Data. ***MODIS (Moderate Imaging Spectro-Radiometer) data.*** MODIS is a satellite sensor on board Terra satellite and Aqua satellite. We downloaded Collection 5.1 Aqua and Collection 5.0 Terra M3 AODs (monthly means of daily means) at 550 nm. Terra AOD and Aqua AOD on the 1° by 1° resolution were converted to monthly combined AOD on the T42 resolution using the following algorithm: If there are at least five values from either satellite in each T42 gridbox, a median is obtained to represent the grid. This algorithm removes outliers automatically.

MISR (Multiangle Imaging Spectro-Radiometer) data. We downloaded the CGAS MIL3MAE.4 product. Out of this monthly product, we selected 555 nm AOD and AOD Ångström exponent (α). The data are originally available on the 1° by 1° resolution, and were converted into the T42 resolution using a median method similar to that adopted for the MODIS AOD. The 550-nm AOD was obtained from the 555-nm AOD and α.

AERONET (Aerosol Robotic Network). AERONET is a ground-based network that reports aerosol optical properties (1). We downloaded the monthly Level 2.0 from Version 2 AERONET product. We use AOD from the direct sun products, although the AERONET SSA and ASY we use are based on an inversion method. AAOD is obtained from the monthly AOD and SSA instead of the AERONET AAOD product. This monthly AERONET AOD/AAOD is used for analyzing BC, OM, and dust optical properties. Where necessary, we logarithmically interpolated AOD and linearly interpolated SSA/ASY to the desired wavelength.

Our technique of identifying the CA AAOD component in AAOD (i.e., Eq. **1**) has nonlinear terms and can thus create biases if monthly AERONET AOD and SSA are used. To quantify the bias, we made the following computation: In this investigation, we used Level 2.0 daily AERONET data to compute monthly AERONET AOD and SSA.

Using monthly data inflates CA AAOD in CA-rich areas (although reducing dust AAOD) and inflates dust AAOD over dusty areas (and reducing CA AAOD). Using monthly data only increases CA AAOD by less than a few percent in CA-rich area, and this increase is counteracted by a decrease in dusty areas. Thus, we conclude that using monthly data will create insignificant global biases.

AERONET AAE is computed using the AAOD at 440, 675, and 870 nm.

Aerosol climatology. Aerosol data was averaged to generate 2001–2009 climatology for each calendar month. AOD was averaged arithmetically. SSA was AOD-weighted and averaged. Climatological AAE was obtained from climatological AAOD.

Observation error. Our empirical estimates of global-averaged CA AAOD and forcing should be subject to observation errors. The observation input for this study is climatological aerosol data. Specifically, the observation input in Eq. **1** is dominated by the AERONET AAOD, given our assimilation scheme. In order for the AERONET AAOD errors to affect our global-averaged estimates, the errors should not be random.

Eck et al. (2) estimated that climatological AERONET SSA differs from in situ measured SSA by up to 0.02; Fig. 14 of their study shows that AERONET SSA tends to be underestimated in low α areas and overestimated in high α areas. Regarding AERONET AOD, the maximum error is between 0.01 and 0.015 for Level 2.0 data (3). A direct validation of AERONET AAOD with UAV observations by Corrigan et al. (4) shows that AERONET AAOD errors are less than 20%.

In order to quantify the uncertainty of our estimates caused by observation error, we digitized Fig. 14 from Eck et al. (2) and capped the SSA error at 0.02. Then, we perturbed AOD by ±0.015. The generated AAOD error is capped at 20% in any grid. The results show that the maximum uncertainty of our global estimates is about 10%.

Data Combination. Eq. **1** is solved for $\tau_{a_{CA}}(\lambda_R)$ and $\tau_{a_D}(\lambda_R)$ at each grid and each calendar month (totaling 12 months) from given $\tau_a(\lambda_R)$ and β. When $\beta < \beta_{CA}$ ($\beta > \beta_D$), β is set to β_CA (β_D); $\tau_a(\lambda_R)$ is calculated by $\tau(\lambda_R) \bullet [1 - \mathrm{SSA}(\lambda_R)]$; and $\tau(\lambda_R)$, $\mathrm{SSA}(\lambda_R)$, and β are the observational input from the 2001–2009 aerosol climatology. Gaps in the observations are filled with the Georgia Tech/Goddard Global Ozone Chemistry Aerosol Radiation and Transport (GOCART) simulation. Here, we explain how we have generated global $\tau(\lambda_R)$, $\mathrm{SSA}(\lambda_R)$, and β values (λ_R denotes 550 nm).

AOD (λ_R). We combine the 2001–2009 averaged MODIS, MISR, and AERONET AODs for each calendar month using the following assimilation process, which takes place in three steps: (*i*) We fill the gaps in MODIS AOD with MISR AOD using the iterative difference-successive correction method developed by Cressman (5). MODIS does not give AOD over desert areas where MISR offers AOD. (*ii*) The remaining gaps in MODIS + MISR AOD are filled with GOCART AOD, again using Cressman's method (5). (*iii*) The spatial pattern in MODIS + MISR + GOCART AOD is coupled with the sparsely distributed AERONET AOD values, using Chung et al.'s technique (6), as below.

$$N_AODj = MMG_AODj \times \frac{\sum_i \frac{AERONETj,i}{dj,i^4}}{\sum_i \frac{MMG_AODj,i}{dj,i^4}}, \qquad \textbf{[S1]}$$

where $N_{\mathrm{AOD}}j$ is the adjusted new value of the AOD at grid j; AERONETj,i is an AERONET_AOD at station location I nearby grid j; dj,i is the distance between j and i; and $\mathrm{MMG_{AOD}}j,i$ is the MODIS + MISR + $\mathrm{GOCART_{AOD}}$ at the grid of AERONETj,i. In this assimilation method, the order of influence is AERONET > MODIS > MISR > GOCART. Final AOD (i.e., N_{AOD}) matches AERONET AOD wherever AERONET AOD exists.

SSA(λ_R). SSA in this study is obtained by integrating AERONET SSA with GOCART SSA. GOCART SSA is computed using GOCART AODs as follows:

$$SSA(\lambda_R) = (0.741 \bullet \tau_{\mathrm{CA}}(\lambda_R) + 0.957 \bullet \tau_{\mathrm{D}}(\lambda_R) + \tau_{\mathrm{rest}}(\lambda_R))/\tau(\lambda_R), \qquad \textbf{[S2]}$$

where 0.957 is dust SSA. This number comes from AERONET SSA over the sites that give AAE around 2.415 (top 5% AAE in the dust AAE distribution). CA SSA of 0.741 is chosen to minimize the global/annual mean difference between GOCART SSA and AERONET SSA.

Then, these GOCART SSAs are further adjusted by AERONET SSA as below:

$$(1 - N_S SAj) = (2 - (1 - G_S SAj) \times \frac{\Sigma_i \frac{1-AERONETj,i}{dj,i^4}}{\Sigma_i \frac{1-G_S SAj,i}{dj,i^4}}. \quad \textbf{[S3]}$$

Like Eq. **S1**, Eq. **S3** maximizes the influence of AERONET data. By applying Eq. **5**, the final SSA has observational constraint on regional scales.

AAE (=β). AAE is obtained by integrating AERONET AAE with GOCART AAE. GOCART AAE is computed using Eq. **1**, which requires the ratio $\tau_{a_{CA}}(\lambda_R) : \tau_{a_D}(\lambda_R)$. This ratio is obtained by $\tau_{CA}(\lambda_R) \bullet 31.0 : \tau_D(\lambda_R)$, where $\tau_{CA}(\lambda_R)$ and $\tau_D(\lambda_R)$ are GOCART-simulated CA and dust AODs. To minimize the global/annual mean difference between GOCART AAE and AERONET AAE, 31.0 is chosen.

Finally, these GOCART AAEs are adjusted by AERONET AAEs, as below:

$$N_A AEj = G_A AEj + \frac{\Sigma_i \frac{AERONETj,i - G_A AEj,i}{dj,i^4}}{\Sigma_i \frac{1}{dj,i^4}}. \quad \textbf{[S4]}$$

By applying Eq. **S4**, the final AAE has observational constraint on regional scales.

CA AAE. CA AAE depends on the ratio of BC to OM, and thus should not be uniform globally. We divide the world into four regions (Fig. S1*B*) to represent presumably different BC/OM ratios. Within each region, we obtain CA AAE that can represent the region. We use a single value to represent the region. Using a single value might create errors in retrieved CA AAOD on scales smaller than the region, but will produce accurate CA AAOD on large and global scales if the CA AAE value correctly represents the regional mean. Because BC, OM, and dust all contribute to AAE, dust-free AAE corresponds to CA AAE.

We calculate region-averaged CA AAE as follows: In each region, we first identify smaller areas with relatively less dust influence. For example, we use northeastern United Stated (85–70° west and 38–44° north), eastern Asia (114–145° east and 31–42° north), and western Europe (5° west–17° east and 44–55° north), areas in the fossil fuel combustion–dominated region. The AERONET AOD and AAOD averaged over the chosen small area at 440, 675, and 870 nm are used to compute area-mean AE and AAE for each calendar month. We then identify calendar months that have at least 10 data and high AE. The AE criterion is to remove dust-influenced months. The chosen months and areas are in the caption of Fig. 1. Then, area-mean calendar month–mean AAEs are averaged for CA AAE in the region.

The Fig. 1 caption does not explain the southern Asia region or the eastern Europe region. There are not enough AERONET data in southern Asia, and so all the available data from October to May are averaged in this region. For the eastern Europe region, the chosen area is 20–45° east and 42–60° north and the chosen calendar months are from March to October.

Empirical Determination of CA ASY. Fig. S2*D* shows the distribution of total aerosol asymmetry parameter (ASY) in the biomass burning–dominated areas, over which carbonaceous aerosols should dominate. The average ASY in the biomass-burning areas is about 0.64, which we use for the baseline CA forcing run. The biomass-burning aerosols include nitrate and sulfate. Because nitrate and sulfate are expected to have bigger particle sizes than BC and OM, pure CA ASY might be lower than 0.64. We conduct a sensitivity test where CA ASY is lowered to 0.55 (i.e., 15% reduction). In this run, CA AE is also set to 1.8 (15% increase) from 1.66. CA AE of 1.66 in the baseline run comes from biomass-burning aerosol average AE.

Monte-Carlo Aerosol Cloud Radiation (MACR) Modeling. We use the MACR model as in Chung et al. (6), who included the effect of observed clouds. To run the model, two additional variables are needed: SSA spectral dependence and vertical profile. CA SSA spectral dependence is obtained by its 550-nm SSA, AAE, and AE. Regarding vertical profile, Zarzycki and Bond (7) demonstrated strong sensitivity of BC forcing to the vertical profile with respect to cloud. Our baseline CA direct radiative effect (DRE) estimate uses a uniform profile in the globe, as in Chung et al. (6). To understand the sensitivity of the CA DRE to vertical profile, we replace the uniform profile in the tropics by what Ramanathan et al. (8) showed from their UAV campaigns in one experiment, and by a Planetary Boundary Layer (PBL)-concentrated profile in another experiment, although we retain the uniform profile in the extratropics in all the experiments (Fig. S3). The CA profile from the UAV campaign in southern Asia cannot represent the global profile. However, using this UAV profile in the entire tropics should set the upper limit. Thus, we argue that the CA forcing range established from these three profiles represents the maximum forcing uncertainty related to vertical profile.

Uncertainty of Our Global Estimates. The uncertainty range given in Table 2 is calculated using the following method: We first choose the parameter change that gives the largest range of the estimate (i.e., from A to B). The uncertainties associated with the other parameter changes are averaged, referred to as $\pm E1$. The observation error is referred to as $\pm E2$. The estimate is then considered to range from $A - \sqrt{E1^2 + E2^2}$ to $B + \sqrt{E1^2 + E2^2}$.

1. Holben BN, et al. (2001) An emerging ground-based aerosol climatology: Aerosol optical depth from AERONET. *J Geophys Res* 106:12067–12097.
2. Eck TF, et al. (2010) Climatological aspects of the optical properties of fine/coarse mode aerosol mixtures. *J Geophys Res* 115:D19205.
3. Eck TF, et al. (1999) Wavelength dependence of the optical depth of biomass burning, urban, and desert dust aerosols. *J Geophys Res* 104:31333–31349.
4. Corrigan CE, Roberts GC, Ramana MV, Kim D, Ramanathan V (2008) Capturing vertical profiles of aerosols and black carbon over the Indian Ocean using autonomous unmanned aerial vehicles. *Atmos Chem Phys* 8:737–747.
5. Cressman GP (1959) An operational objective analysis system. *Mon Weather Rev* 87:367–374.
6. Chung CE, Ramanathan V, Kim D, Podgorny IA (2005) Global anthropogenic aerosol direct forcing derived from satellite and ground-based observations. *J Geophys Res* 110:D24207.
7. Zarzycki CM, Bond TC (2010) How much can the vertical distribution of black carbon affect its global direct radiative forcing? *Geophys Res Lett* 37:L20807.
8. Ramanathan V, et al. (2007) Warming trends in Asia amplified by brown cloud solar absorption. *Nature* 448:575–578.

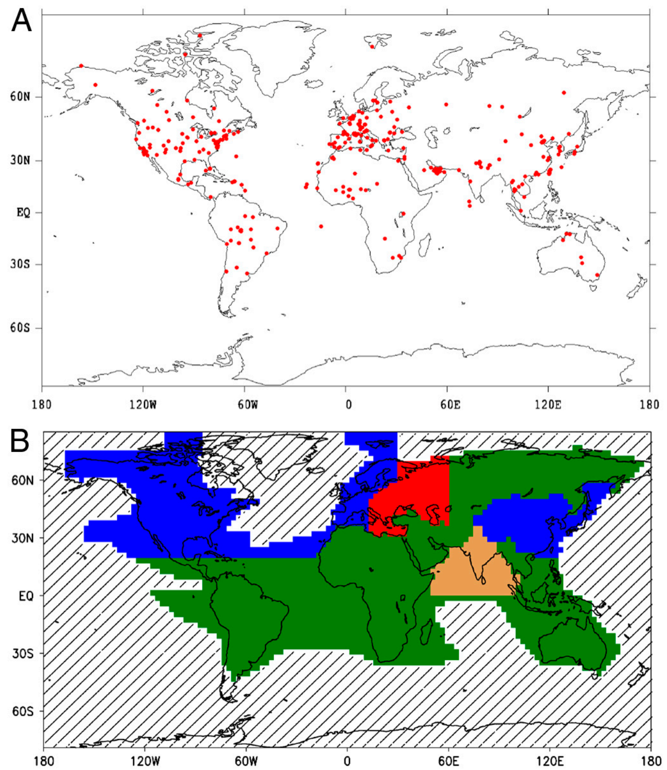

Fig. S1. (*A*) Locations of monthly AERONET data that give both AOD and SSA between 2001 and 2009. There are 317 such AERONET stations that give both AOD and SSA (AERONET Level 2.0). (*B*) Division of the world in terms of CA AAE. The divided regions are: fossil fuel combustion (blue), biomass burning (green), southern Asia (dark yellow), and eastern Europe (red). The hatching shows the area where the SSA(λ_R) and β input in Eq. **1** are dominated by the GOCART simulation, because AERONET gives very little influence over this area. Over the hatched area, CA AAE is taken from the upstream CA AAE over land.

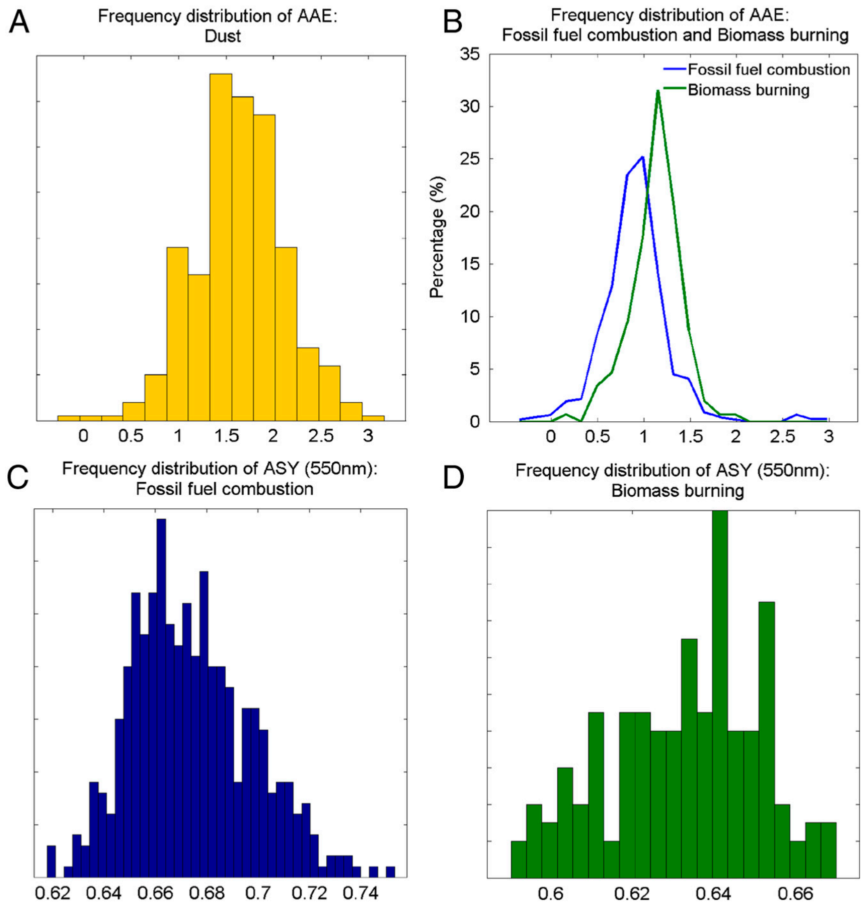

Fig. S2. AERONET data analysis. Monthly data (instead of 2001–2009 averages) from 2001 to 2009 are used. (*A*) Frequency distribution of (pure or polluted) dust AAE. To compute dust AAE, we select the AERONET data when AE <0.3. Thus, pure dust, polluted dust (e.g., BC-contaminated dust), and sea salt mixed with minor CA are all shown here. Because BC always accompanies OM, polluted dust is basically dust with CA. High AAE values should represent pure dust, because the presence of CA lowers AAE. (*B*) Frequency distribution of CA AAE in terms of percentage. AERONET data are classified into fossil fuel or biomass burning–dominated kind if the area and calendar month correspond to those in the caption of Fig. 1. (*C*) Frequency distribution of AERONET asymmetry parameter (ASY) at 550 nm for fossil fuel combustion–dominated aerosols. (*D*) Frequency distribution of AERONET ASY at 550 nm for biomass burning–dominated aerosols.

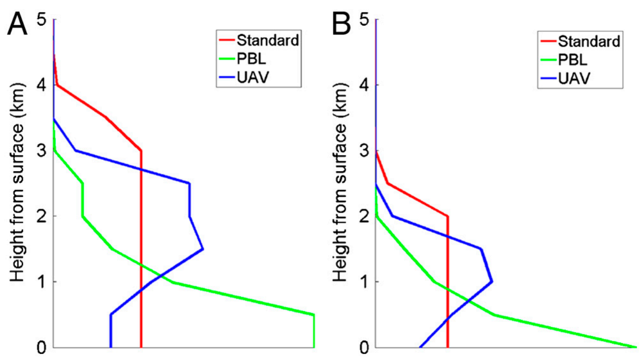

Fig. S3. Three CA vertical profiles in the tropics (30° south–30° north) as in the MACR model. The model vertical resolution is 0.5 km. Profiles get shrunken as the surface altitude rises (as in Chung et al. 6). The profiles on the left are over the ocean, and those on the right are over the 1.5-km altitude surface.

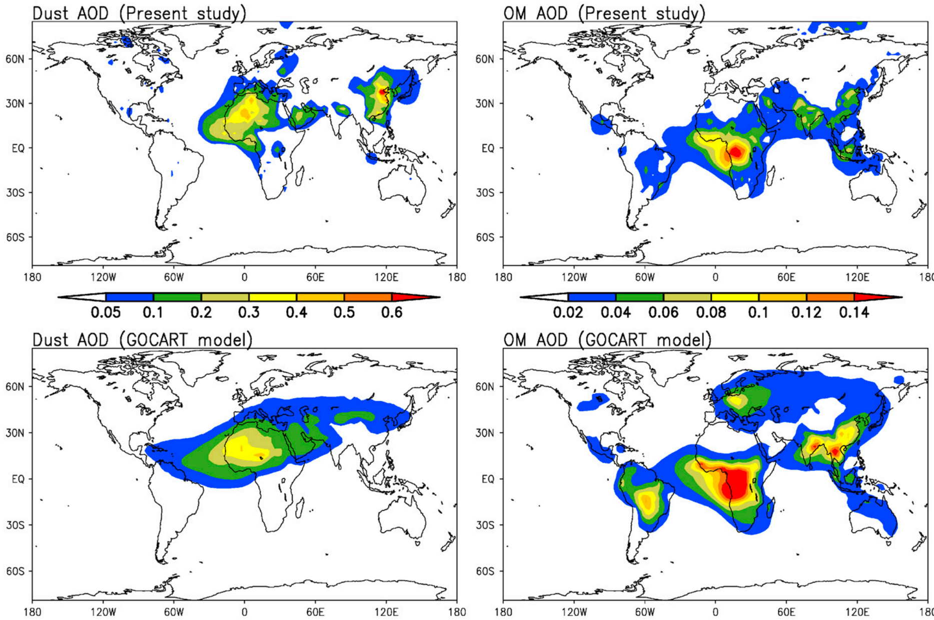

Fig. S4. Comparing our AOD estimates with AOD simulation by GOCART model. All are for annual mean.

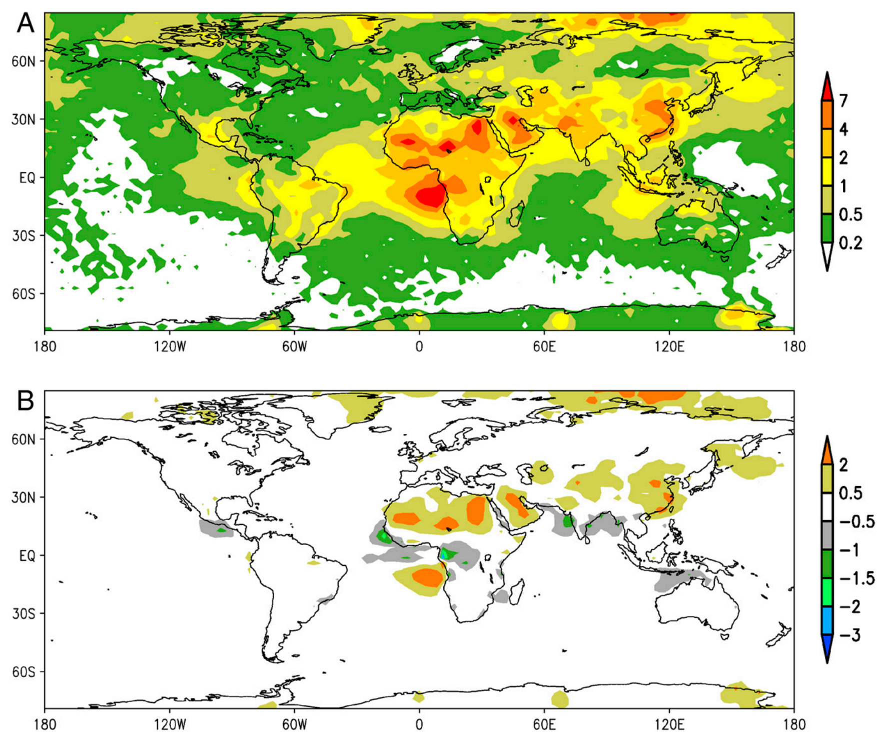

Fig. S5. CA DRE sensitivity experiment. (*A*) Annual mean CA TOA DRE estimate from the baseline run. (*B*) CA DRE estimate with the GOCART magnitude of $AOD_{BC}(\lambda_R)$ and $AOD_{OM}(\lambda_R)$, and OM SSA of 1.0. In the run shown in *B*, our $AOD_{BC}(\lambda_R)$ is scaled by $\times$ 0.63 and our $AOD_{OM}(\lambda_R)$ is scaled by $\times$ 1.56 in order to match global-averaged GOCART $\tau_{BC}(\lambda_R)/\tau_{OM}(\lambda_R)$.

Table S1. Comparing the present study with the two previous semiempirical studies

	Semiempirical calculation by Sato et al. (1)	Semiempirical calculation by Ramanathan and Carmichael (2)	Empirical calculation by the present study
Global BC DRE	$+1.0\ Wm^{-2}$	$+0.9\ Wm^{-2}$	$+0.75\ Wm^{-2}$
Global aerosol observation input	AERONET AAOD at multiple wavelengths	MODIS AOD and AERONET AOD/SSA, all at 550 nm	MODIS AOD and MISR AOD at 550 nm; AERONET AOD/SSA at multiple wavelengths
Diagnosing BC component	(*i*) Solving for BC, OM and dust simultaneously with (*ii*) BC/OM/dust absorptions at multiple wavelengths that were calculated with spherical shape assumption, prescribed size distribution, and refractive index; (*iii*) OM AAE of 3.2.	Based on GOCART-simulated ratio of BC AOD:dust AOD:total AOD.	(*i*) Solving for CA AAOD and dust AAOD first, and then dividing CA between BC AAOD and OM AAOD, in order to assure the accuracy of retrieved OM AAOD (because dust and OM have similar spectral dependence of absorption); (*ii*) BC and dust AAE obtained by AERONET AAOD analysis instead of computing them with assumed sizes and refractive indices.
BrC AAOD	No explicit treatment of BrC	OM assumed to be 100% scattering, thus no BrC; because total aerosol absorption was constrained by AERONET, BrC AAOD was included as part of BC AAOD.	BrC AAOD = OM AAOD at 550 nm
Deriving global BC pattern	100% from aerosol-simulation models	Jointly from aerosol observations and GOCART simulation	Mostly from aerosol observations

1 Sato M, et al. (2003) Global atmospheric black carbon inferred from AERONET. *Proc Natl Acad Sci USA* 100:6319–6324.

2 Ramanathan V, Carmichael G (2008) Global and regional climate changes due to black carbon. *Nat Geosci* 1:221–227.

Table S2. β_CA in the present study

	Fossil fuel-dominated areas: N. America, W. Europe, E. Asia	Eastern Europe	S. Asia	Biomass burning-dominated areas
Dust-free AAE (β_CA)	0.84	0.97	1.16	1.14

Fig. S1*B* shows the definition of the regions.

Table S3. Various global mean CA DRE estimates in units of Wm^{-2}

	TOA forcing	Atmosphere forcing	Surface forcing
Baseline model run	0.80	3.88	−3.08
Modification to baseline: UAV profile	0.79	3.87	−3.08
PBL-concentrated profile	0.61	3.68	−3.08
Dust AAE: 2.63	0.81	3.92	−3.11
Dust AAE: 2.212	0.78	3.83	−3.04
OM SSA(λ_R): 0.8	0.88	3.86	−2.98
OM SSA(λ_R): 0.9	0.63	3.91	−3.27
BC SSA(λ_R): 0.3	0.76	3.89	−3.13
BC AAE: 0.67; OM AAE: 6.0	0.89	3.85	−2.96
BC AAE: 0.38; OM AAE: 3.9	0.70	3.90	−3.19
CA AE: 1.8; CA ASY(λ_R): 0.55	0.73	3.88	−3.15
Central value (median of the above) (after round-off)	***0.75***	3.8	−3.05

All the runs meet the constraints imposed by total aerosol observations. Baseline run uses the following parameters: $B_D = 2.415$; $\beta_{BC} = 0.50$; $\beta_{OM} = 4.8$; $SSA_{BC}(\lambda_R) = 0.19$; $SSA_{OM}(\lambda_R) = 0.85$; $\alpha_{CA} = 1.66$; $ASY_{CA} = 0.64$. Aerosol profile in the baseline run is as in Chung et al. (6). Cloud effects are included in all the runs as in Chung et al. (6).

Table S4. Various BC DRE and OM DRE estimates

Various BC DRE estimates*	TOA forcing	Atmosphere forcing	Surface forcing
Baseline model run	0.77	2.72	−1.95
UAV profile	0.77	2.72	−1.95
PBL profile	0.64	2.60	−1.96
BC AAE: 0.67; OM AAE: 6.0	0.80	2.90	−2.10
BC AAE: 0.38; OM AAE: 3.9	0.74	2.59	−1.85
Various OM DRE estimates†	TOA forcing	Atmosphere forcing	Surface forcing
Baseline model run	0.03	1.16	−1.13
UAV profile	0.02	1.15	−1.13
PBL profile	−0.03	1.09	−1.12
BC AAE: 0.67; OM AAE: 6.0	0.09	0.95	−0.86
BC AAE: 0.38; OM AAE: 3.9	−0.04	1.31	−1.35
OM SSA(λ_R): 0.8	0.12	1.14	−1.03
OM SSA(λ_R): 0.9	−0.15	1.17	−1.32

*Baseline run uses the following parameters: $B_D = 2.415$; $\beta_{BC} = 0.50$; $\beta_{OM} = 4.8$; $SSA_{BC}(\lambda_R) = 0.19$; $\alpha_{BC} = 1.66$; $ASY_{BC} = 0.64$.

†Baseline run uses the following parameters: $B_D = 2.415$; $\beta_{BC} = 0.50$; $\beta_{OM} = 4.8$; $SSA_{OM}(\lambda_R) = 0.85$; $\alpha_{OM} = 1.66$; $ASY_{OM} = 0.64$.